Journal of Imaging Science and Technology® 54(4): 040502–040502-9, 2010.

Spectral Analysis of Omnidirectional Illumination in a Natural Scene

Shoji Tominaga▲, Atsushi Matsuura and Takahiko Horiuchi▲
Division of Information Sciences, Graduate School of Advanced Integration Science, Chiba University, 1-33 Yayoi-cho, Inage-ku, Chiba 263-8522, Japan
E-mail: shoji@faculty.chiba-u.jp

Abstract. *This article describes a method for analyzing omnidirectional color signals in a natural scene, which contains direct illuminations of daylights and indirect illuminations of the reflected lights from different object surfaces. A multiband omnidirectional imaging system is used for capturing high resolution images in the omnidirectional observations at a particular point in a natural scene. The spectral-power distributions of color signals are recovered from the captured six-band images. The authors investigate the spectral composition of the omnidirectional scene illumination based on the principal component analysis of the whole set of color signals acquired at the same location in a fixed time of day in five months of a year. It is found that all the omnidirectional color signals can be expressed in a linear combination of only three principal components. This property has the potential for high data compression. Moreover, the authors analyze the chromaticity distribution of omnidirectional color signals. Experimental results are presented for omnidirectional color signals obtained in an outdoor scene of university campus. The reliability of the proposed method is examined from various points of view. An application to image rendering is shown.* © *2010 Society for Imaging Science and Technology.*
[DOI: 10.2352/J.ImagingSci.Technol.2010.54.4.040502]

INTRODUCTION

Spectral analysis of a natural scene is definitely one of the most important areas of research in the recent field of color imaging science and technology. Some representative works on the spectral analysis are listed in Refs. 1–8. These works are mainly classified into two types of analysis: (1) surface-spectral reflectances as physical properties of materials and (2) daylight spectra as effects of natural light. Historically, the properties of reflectance spectra of natural and artificial objects were investigated by many researchers, such as Krinov,[9] Malony,[10] Parkkinen et al.,[11] and Vrhel et al.[12] Recently, reflectance spectra in forests and coral reefs were investigated by Chiao et al.,[1] in which a multispectral imaging device was used to sample the spectra from many locations in a single scene. Concerning daylight spectra, the article by Judd et al.[8] is well known as a historical work, where most daylight spectra could be estimated by linearly combining the mean spectrum and two basis functions. Chiao et al.[2] analyzed natural illuminants in the forest, where the images of white cardboard were captured by a color camera. Recently, Hernández-Andrés et al.[5] analyzed a large set of hemispheric daylight spectra measured during two years in southern Europe. Kohonen et al.[7] introduced useful databases for different surfaces and daylight.

However, these previous works are limited to spectral analysis of object surfaces sampled in natural scenes and of daylight at specific areas in a scene of interest like a sky. It should be noted that the light source forming color images in a natural scene is not a single light source, but a mixture of a point light source such as sunlight and of an area light source with a spatially changing spectral distribution. Moreover, note that an object surface in a natural scene is illuminated not only by such a light source but also by all the reflected lights from the surrounding object surfaces. Spectral analysis based on omnidirectional observations in a natural scene was not considered so far.

There are many studies in the literature that use a mirror-like ball to estimate the illumination in natural scenes.[13–15] Debevec[13] developed a technique using a mirrored ball in computer graphics called a light probe. He captured color images of an omnidirectional scene and created the images of synthetic objects in the real scene. The image rendering was based on RGB color values. Dror et al.[14] studied the statistical properties of real-world illumination for facilitating the understanding of human material perception. The regularity and variability of illumination patterns were examined using distributions of illumination intensities. Tominaga et al.[15] proposed a method for estimating an omnidirectional distribution of the scene illuminant spectra. This kind of system using a mirrored ball, however, has several problems, such as low and non-uniform spatial resolution and a dead region due to imaging the camera itself.[16]

The present article describes a method for analyzing omnidirectional spectra in a natural scene, which contains direct illuminations of different light sources from the sky and indirect illuminations of the lights reflected from different object surfaces. The spatial distribution of illuminations is obtained from omnidirectional observations at a particular point of a natural scene. A multiband omnidirectional imaging device is used for capturing high resolution images in the omnidirectional observations. The spectral-power distributions for both the direct and indirect illuminations that reach the imaging system are called the color signals in this

▲IS&T member.

Received Sep. 20, 2009; accepted for publication Apr. 14, 2010; published online Jun. 9, 2010.
1062-3701/2010/54(4)/040502/9/$20.00.

article. The spectral composition of the omnidirectional illumination is investigated based on the principal component analysis (PCA) of the set of color signals recovered from the captured multiband images. Next, we analyze the omnidirectional color signals obtained at a fixed place over different seasons of a year. Several basis functions of the spectral components are extracted from the PCA of the whole set of color signals. Then, it is found that all the omnidirectional color signals can be expressed in a linear combination of a small number of spectral bases. Our analysis suggests that the estimated spectra of omnidirectional illumination have the potential for high data compression.

Moreover, we analyze the chromaticity of omnidirectional color signals. It is known that daylight illuminants are characterized by correlated color temperature. However, because natural real-world illumination includes indirect illumination, the chromaticities of color signals do not always fall on the chromaticity locus of blackbody radiator. The set of color signals must include season characteristics of the natural scene. In this sense the chromaticity analysis is meaningful.

The remainder of this article is organized as follows: we first present the image acquisition technique using a multiband imaging system to measure omnidirectional color signals. Second, we describe the analysis methods. The spectral-power distributions of color signals are recovered via a Wiener estimator from the multiband images. The PCA analysis is applied to the spectral data set for approximating the detailed shape of spectral distributions. The chromaticity distribution of color signals is also analyzed. Third, we present experimental results for omnidirectional color signals obtained in an outdoor scene of a university campus. The reliability of the proposed method is examined from various points of view. An application to image rendering is shown.

MEASUREMENTS

Imaging System

Figure 1 shows a measuring system for acquiring ambient light properties at an arbitrary location in a natural scene. We use an imaging system for capturing multiband omnidirectional images and a spectroradiometer for directly acquiring illuminant spectral-power distribution in a particular direction. The imaging system is realized with a trichromatic digital camera, a fisheye lens, color filters, and a rotating table (see Ref. 16 for the details). The camera is a Canon EOS camera with the image size of 4082×2718 pixels and the bit depth of 12 bits. The fisheye lens is a SIGMA circular fisheye lens based on the equi-solid-angle projection. Two additional color filters with different characteristics of spectral transmittance are used for multispectral image acquisition. Each filter is placed between the lens and the camera body. Combining these color filters to the original camera spectral sensitivities leads to different sets of trichromatic spectral sensitivity functions. Therefore, two sets of the modified trichromatic spectral sensitivities result in an imaging system with six spectral bands. Figure 2 shows the

Figure 1. Measuring system for acquiring ambient light properties.

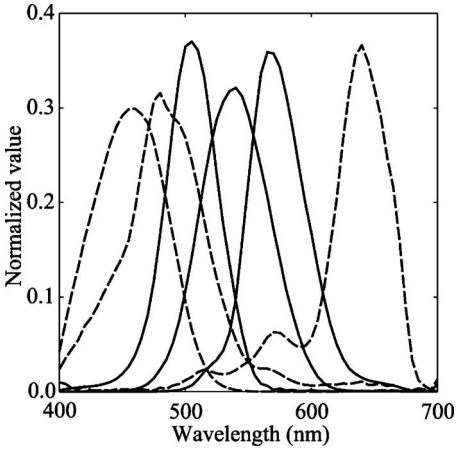

Figure 2. Spectral sensitivity functions of the imaging system.

overall spectral-sensitivity functions of the present multispectral imaging system.

Since the present fisheye system takes pictures of a scene in a hemisphere, we need at least two sets of images in opposite viewing directions for completing an omnidirectional image. To eliminate a certain distortion at the edge of the image plane, we can combine three sets of images observed at rotation angle intervals of 120°.

Collections of Omnidirectional Images

The collections of omnidirectional images were conducted on campus in Chiba University for a one year duration during 2008–2009. There are four seasons in Japan. Each of the four seasons has its characteristics of the natural scene. In principle the spectral compositions of omnidirectional color signals are acquired at a particular location change depending on the seasons. The multiband omnidirectional images with six-spectral channels were captured at the same location at a fixed time of morning in April (spring) 2008,

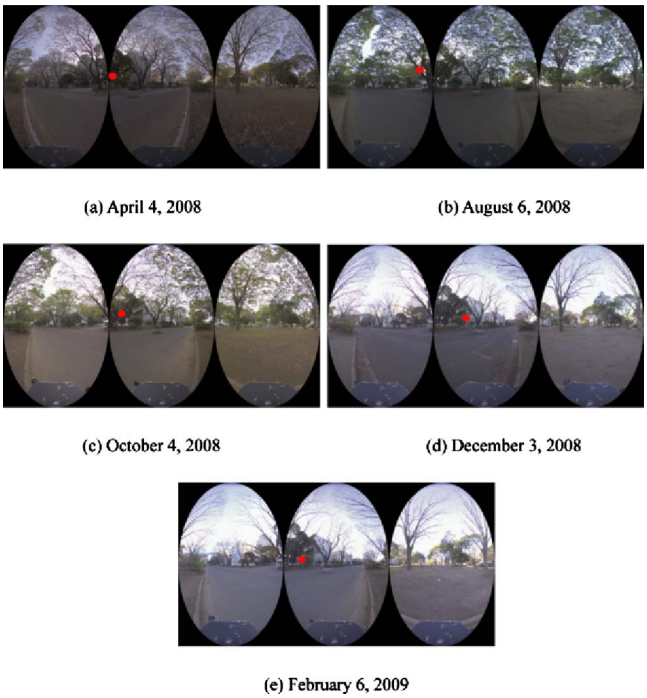

Figure 3. Omnidirectional images captured with the 120° visual field in different seasons. (a) April 4, 2008, (b) August 6, 2008, (c) October 4, 2008, (d) December 3, 2008, and (e) February 6, 2009. Each red dot indicates the solar position behind buildings.

August (summer) 2008, October (autumn) 2008, December (winter) 2008, and February (winter) 2009. The weather of all the days was clear. A set of three images during each day were captured with the 120° visual field at three horizontal directions. Figure 3 shows the color images, converted from the original six-band images acquired in different seasons. The camera was held at about 1 m above the ground. The scenes contain direct illuminations from the sky and indirect illuminations from the surrounding various object surfaces. Table I lists the measurement dates and the solar positions with azimuth and elevation angle. In Fig. 3, each red dot indicates the solar position in the corresponding image. Because the omnidirectional images were captured soon after the sunrise, the sun is hiding behind buildings in the images.

Even if they do not include strong sunlight, the range of light intensities in a natural scene is very large so that the image intensities vary greatly on pixels. In the present image acquisition, 15 images of the same scene were taken with the camera at shutter speeds of 2, 1, 1/2,…, 1/8000 s, which were combined into high dynamic range (HDR) images with 22 bits. The omnidirectional image is composed of three HDR images obtained at three directions with the separation of 120° as shown in Fig. 3.

We can see seasonal characteristics of the natural scene. The cherry blossom of the image in April is a feature of spring time. The second image in August reflects the season of green leaves. The images in winter are characterized by dry vegetation.

Table I. Measurement dates and the solar positions.

Measurement date	Azimuth	Elevation angle
2008/04/04 6:22	97.8	15.4
2008/08/06 5:51	84.8	22.8
2008/10/04 6:37	109.3	11.5
2008/12/03 7:32	129.6	7.3
2009/02/06 7:35	122.2	8.6

ANALYSIS METHODS

Estimation of Color Signals

Omnidirectional color signals to be estimated are not only direct illuminations from light sources around the observation point but also indirect illuminations of the lights reflected from all the surrounding object surfaces. The observed images can include various noise on sensors and optical process. The image sensor outputs are modeled as a linear system

$$\rho_i = \int_{400}^{700} E(\lambda) R_i(\lambda) d\lambda + n_i, \quad (i = 1,2,\ldots,6), \qquad (1)$$

where $E(\lambda)$ is the color signal, $R_i(\lambda)$ is the spectral sensitivity function of the ith sensor, and n_i is the noise component with zero mean. We sample each spectral function at n points with an equal interval $\Delta\lambda$ in [400, 700 nm]. Let $\mathbf{e}$ be an n-dimensional column vector representing the color signal $E(\lambda)$ and let $\mathbf{R}$ be a $6\times n$ matrix with the element $r_{ij}=R_i(\lambda_j)\Delta\lambda$. Moreover, define a six-dimensional column vector $\boldsymbol{\rho}$ representing a set of the sensor outputs ρ_i. Then the above imaging relationships are summarized in a linear matrix equation

$$\boldsymbol{\rho} = \mathbf{Re} + \mathbf{n}. \qquad (2)$$

When the signal $\mathbf{e}$ and the noise $\mathbf{n}$ are uncorrelated, the Wiener estimate $\hat{\mathbf{e}}$ is given as

$$\hat{\mathbf{e}} = \mathbf{C}_{ss}\mathbf{R}^t(\mathbf{R}\mathbf{C}_{ss}\mathbf{R}^t + \boldsymbol{\Sigma})^{-1}\boldsymbol{\rho}, \qquad (3)$$

where $\mathbf{C}_{ss}$ is the correlation matrix of illumination signals $\mathbf{C}_{ss}=\mathbf{E}[\mathbf{e}\mathbf{e}^t]$ and $\boldsymbol{\Sigma}$ is the covariance matrix of noises $\boldsymbol{\Sigma}=\mathbf{E}[\mathbf{n}\mathbf{n}^t]$. We can assume that the noises in each spectral channel are statistically independent. In this case, the covariance matrix is reduced to be diagonal as $\boldsymbol{\Sigma}=\mathrm{diag}(\sigma_1^2,\sigma_2^2,\ldots,\sigma_6^2)$. In the real computation of spectral estimation, each spectral-power distribution is usually sampled at 61 equally spaced wavelength points as $n=61$.

The noise component includes image sensor noises based on thermal noise and shot noise and an approximation error in the model. Although estimation of the noise properties is not easy, there are some proposals to do this. Shimano[17] proposed a method for estimating the noise covariance $\boldsymbol{\Sigma}$ by evaluating the error of spectral reflectance estimates in the spectral domain. However, this method is computationally complicated and rather tedious. Since the

Table II. Set of object surfaces measured on campus.

Object name	Number of measurement points
Green leaves	448
Dead leaves	34
Tree trunks	265
Flower petals	8
Stones	9
Soil ground	53
Asphalt ground	25
Concrete ground	12
Pavement tiles	5
Building walls	12

correlation matrix is based on the relative intensity of the illuminant spectral-power distribution, we only need the signal-to-noise ratio (SNR) of the present imaging system. In this article, we determined the SNR in an empirical way, where the Macbeth Color Checker and several light sources including an incandescent lamp were used as the known object surfaces and light sources. We changed the values of SNR so as to minimize the estimation error of surface-spectral reflectance. Then the SNR corresponding to the minimum error was adopted for the present imaging system.

Sample Data

The Wiener estimator relies upon the statistics of a data set to achieve the estimation. To determine the correlation matrix $\mathbf{C}_{ss}$ properly, we need a large database of scene illumination, which is composed of the direct illuminations and the indirect illuminations. For this purpose we created two spectral data sets for surface-spectral reflectances and light sources.

Concerning the surface reflectance, we collected many objects from the real world of our campus and measured the surface-spectral reflectances by a spectrophotometer. Also we measured the surface-spectral reflectances of many large objects by using the spectroradiometer and a white reference sample. Table II lists the whole set of surface reflectances measured from different objects on campus. The constitution of objects and the combination of the number of measurement points reflect the real scenes to be analyzed in this article. The set of 871 samples are representatives of the type of object surfaces that we are measuring with the camera. Figure 4(a) shows the set of spectral reflectance curves of 871 object surfaces.

Concerning the light source, we used the CIE standard illuminants with different correlated color temperatures from 5000 to 10,000 K.[18] These illuminants approximate the real light sources in daytime. Moreover, a small number of the direct measurements of the sky were added to the light source set. Fig. 4(b) shows the spectral distributions of nine light sources.

Next, we produced a large database of about 8000 color signals by multiplying the surface-spectral reflectances and

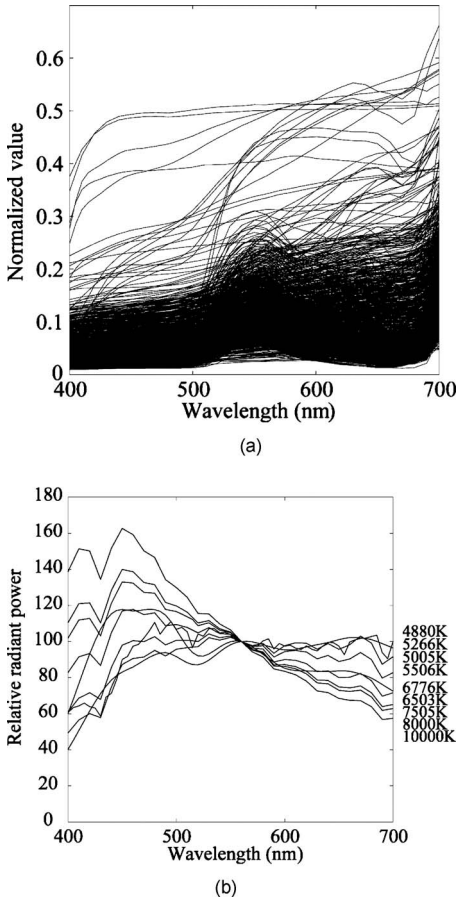

Figure 4. Databases of surface-spectral reflectances for a variety of objects on university campus and spectral-power distribution for nine light sources. (a) Reflectances and (b) light sources.

the light source spectra. The ratio of indirect illuminations and direct illuminations was estimated by the ratio that the sky occupied in the omnidirectional images. Therefore, 100 sets of light sources in Fig. 4(b) were combined to the above indirect illumination set of color signals to complete the whole color signal database.

PCA of Color Signals

The PCA analysis is applied to the whole set of color signals obtained for an omnidirectional scene. This analysis is done in the original observation coordinate system of the equi-solid-angle projection. The omnidirectional image is represented with the azimuth angle θ and the rotational angle ϕ. The spectral distribution of color signal $\mathbf{e}$ is a function of θ and ϕ. The estimate $\hat{\mathbf{e}}(\theta,\phi)$ is calculated using Eq. (3) from the sensor outputs at the corresponding pixel. A singular value decomposition (SVD) of the set of $\hat{\mathbf{e}}(\theta,\phi)$ provides that each color signal can uniquely be expressed in a linear combination of the n orthogonal vectors as

$$\hat{\mathbf{e}}(\theta,\phi) = c_1(\theta,\phi)\mathbf{u}_1 + c_2(\theta,\phi)\mathbf{u}_2 + \cdots + c_n(\theta,\phi)\mathbf{u}_n, \quad (4)$$

where $\{\mathbf{u}_1, \mathbf{u}_2, \ldots, \mathbf{u}_n\}$ are the left singular values. Because the observation space is six dimensional, n is limited to six as a practical matter.

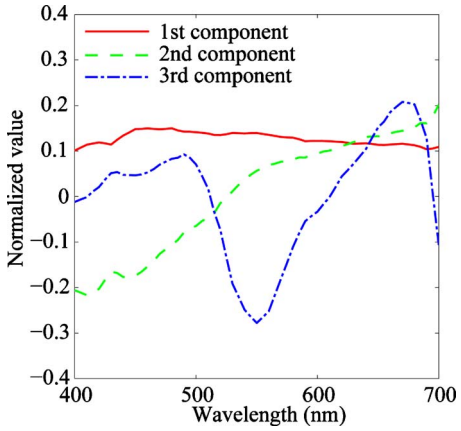

Figure 5. Three principal components for the color signal database.

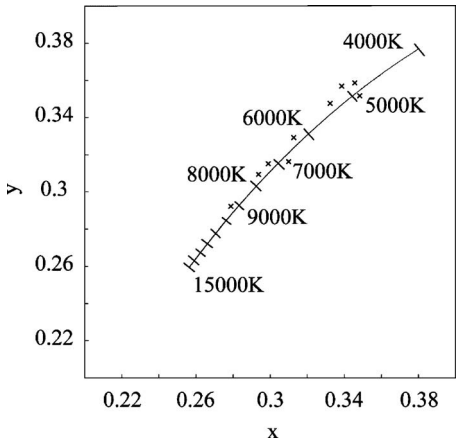

Figure 6. Chromaticity locus of blackbody radiator and chromaticities of daylight spectra.

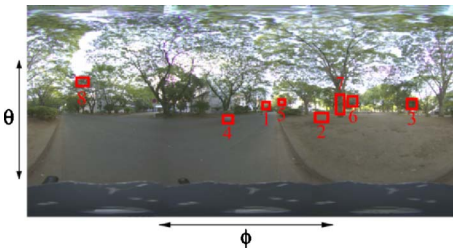

Figure 7. Omnidirectional image of August in the polar coordinates.

Consider an approximate representation of the color signals in terms of some component vectors chosen from $\mathbf{u}_1, \mathbf{u}_2, \ldots, \mathbf{u}_n$. The performance index of the chosen principle components is given by the percent variance $P_K = \Sigma_{i=1}^{K} \mu_i^2 / \Sigma_{i=1}^{n} \mu_i^2$, where $\{\mu_1, \mu_2, \ldots, \mu_n (\mu_i > \mu_{i+1})\}$ are the singular values of the matrix of all $\hat{\mathbf{e}}(\theta, \phi)$. When we choose the first K components, all color signals are represented as

$$\hat{\mathbf{e}}_K(\theta, \phi) = c_1(\theta, \phi)\mathbf{u}_1 + c_2(\theta, \phi)\mathbf{u}_2 + \cdots + c_K(\theta, \phi)\mathbf{u}_K. \tag{5}$$

Because the basis functions of principal components are common to all the color signals, the set of spectral data represented by the high-dimensional vectors are reduced to the set of a small number of coefficients $\{c_i\}$. Thus the spectral image data are compressed. This approximation is optimal in a least square sense. Figure 5 shows the spectral curves of the first three principal components for the whole database of color signals created for simulation experiments in the previous subsection. In this case, the percent variances are $P_1 = 0.967$ for use of the first component only, $P_2 = 0.995$ for the first two components, and $P_3 = 0.998$ for the first three components.

The linear model representation of color signals is determined for the respective omnidirectional scenes in Fig. 3. It should be noted that an appropriate model dimension depends on spectral content in the objective scene. As the performance index, we use the root-mean squared error (RMSE) $E_K = (\mathbf{E}\|\mathbf{e} - \hat{\mathbf{e}}_K\|^2)^{1/2}$ as well as the percent variance. A color difference is also effective as a colorimetric quality metrics. Here we use the CIE 1976 $L^*a^*b^*$ system to calculate the color difference. An effective linear model representation of omnidirectional color signals through one year is selected from the standpoint of data compression and estimation accuracy.

Characterization of Chromaticity

Judd et al.[8] demonstrated that the spectral distribution of daylight is well characterized by correlated color temperature, which led to the CIE standard illuminants. The chromaticity coordinates of nine light sources used in our database are plotted in the CIE 1931 *xy*-chromaticity diagram as shown in Figure 6, where the solid curve indicates the Planckian locus (chromaticity locus of blackbody radiator). The chromaticities of the light sources lie closely on the locus. However, these light sources represent light only under open sky. Chiao et al.[2] investigated the chromaticity loci of natural illuminant spectra measured in forests. The loci of their illuminant spectra shifted toward the green side of the diagram.

Our omnidirectional color signals represent all lights recovered from images captured at a particular point in the outdoor scene. We compute the CIE-*xy* chromaticity coordinates at every pixel of the observed image. The two-dimensional chromaticity loci, called the chromaticity histogram, characterize the chromaticity distribution of the entire scene. The chromaticity loci in omnidirections are distributed in a wider area including daylight spectra and forest illuminant spectra. It should be noted that the number of pixels on the (x, y) coordinates corresponds to the area in the (θ, ϕ) coordinates of the real scene because the present omnidirectional imaging system is based on the equi-solid-angle projection.

EXPERIMENTAL RESULTS

Color Signals

An omnidirectional image was created by combining three partitioned images in Fig. 3 into a latitude/longitude image in a polar coordinate system in order to make a spatial map of omnidirectional color signals. Figure 7 shows the omni-

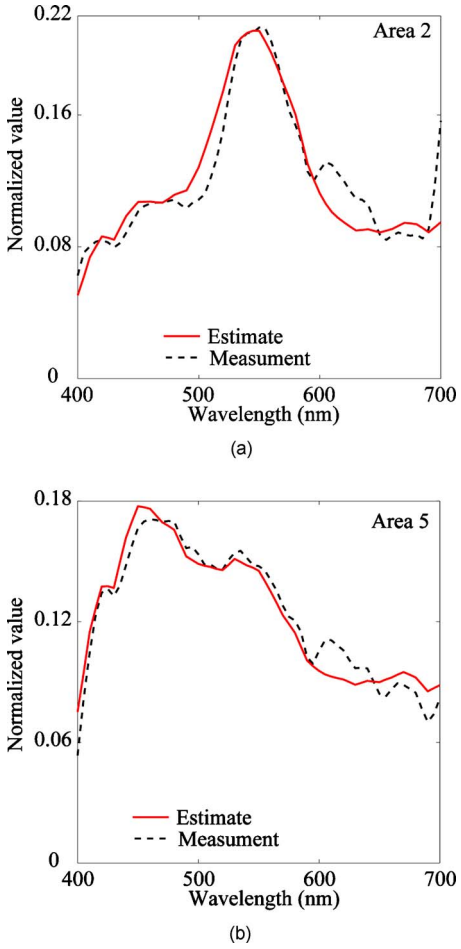

Figure 8. Estimation results of color signals from area 2 and area 5.

directional image of August in the polar coordinate system, where the rectangles indicate test areas of estimation accuracy. The 61-dimensional color signal vector **e** was estimated from the camera data at each pixel of the omnidirectional image by using the algorithm of Eq. (3).

The accuracy of the estimated color signals $\hat{\mathbf{e}}$ was examined for eight areas in Fig. 7. Figure 8 shows the estimation results of color signals from area 2 and area 5 in the scene. We measured directly the color signals reflected from objects in each area by using the spectro-radiometer. The numerical error was calculated between the normalized spectral curves of the estimate $\hat{\mathbf{e}}$ and the measurement $\mathbf{e}_m$ as the RMSE $E=(\mathbf{E}\|\mathbf{e}_m-\hat{\mathbf{e}}\|^2)^{1/2}$, where $\|\mathbf{e}_m\|^2=\|\hat{\mathbf{e}}\|^2=1$. The second column in Table III lists the estimation error in RMSE. The third column lists the CIE-L*a*b* color difference. The comparisons between the estimates and the measurements suggest the accuracy of the present estimation method.

Principal Components

The principal components of color signals for the respective omnidirectional scenes were extracted from SVD of the data set of the estimated color signals $\hat{\mathbf{e}}$. Four figures in Figure 9 show the spectral curves of the first four principal components. Each figure contains five spectral curves belonging to the same rank of principal component in five different

Table III. Estimation errors of color signals for the rectangular areas in Fig. 7.

	$(\mathbf{e}_m-\hat{\mathbf{e}})$		$(\mathbf{e}_m-\hat{\mathbf{e}}_3)$	
Area number	RMSE	ΔE*ab	RMSE	ΔE*ab
1	0.019	5.20	0.022	8.93
2	0.017	5.81	0.017	4.15
3	0.021	5.61	0.021	2.45
4	0.008	4.28	0.009	5.65
5	0.012	5.88	0.014	7.48
6	0.016	4.27	0.019	9.35
7	0.006	3.19	0.006	2.75
8	0.023	5.00	0.023	4.39

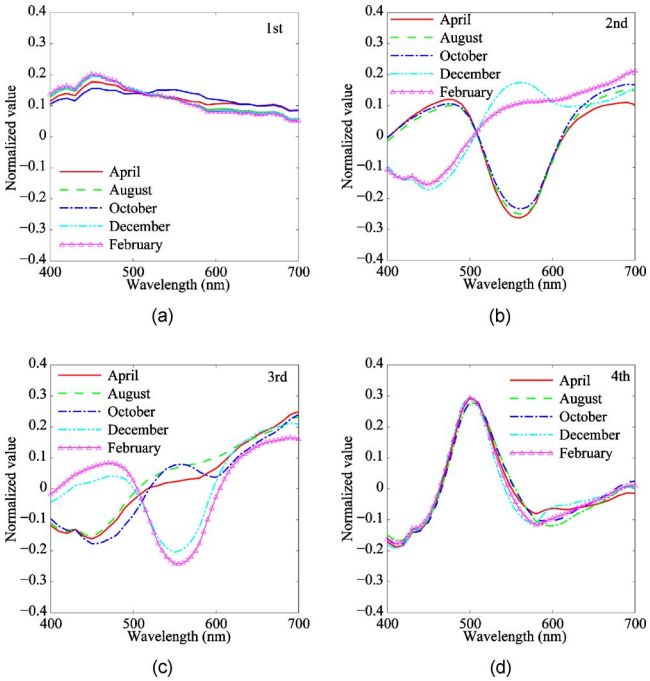

Figure 9. Spectral curves of the first four principal components. (a) First component, (b) second component, (c) third component, and (d) fourth component.

months. We see in Figs. 9(a) and 9(d) that the spectral curves of the first and fourth principal components are close to each other in different months. The detailed comparison between Figs. 9(b) and 9(c) suggests that the second component curve and the third one of December and February are different from the components of the other seasons. Moreover, we should note that the spectral curves in winter in Fig. 9(b) are close to the curves in the other seasons in Fig. 9(c), and in the same way, the spectral curves in winter in Fig. 9(c) are close to the ones in the other seasons in Fig. 9(b). In the winter, dry leaves fall to the ground and so the visible area of the sky increases, while in the other seasons the sky is mostly covered with green leaves and cherry flowers. The second and third components may relate to the sky and leaves. We should note that the four spectral curves

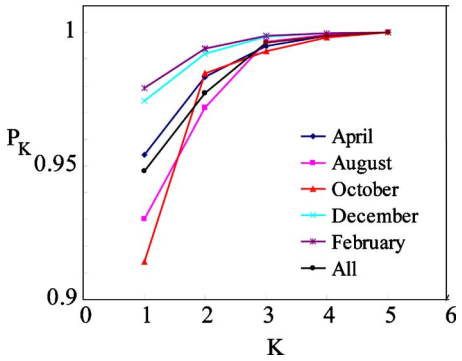

Figure 10. Performance indices P_K for approximation by principal components.

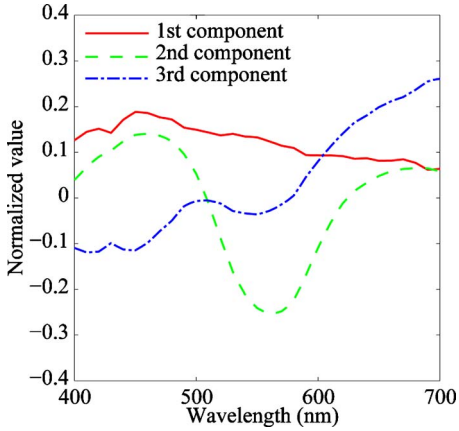

Figure 11. Three principal components for all omnidirectional scenes.

have similar shapes through all seasons, which can describe all omnidirectional color signals.

We calculated the performance indices P_K for use of the first K principal components for the respective months. Figure 10 depicts the performance indices as a parameter of the number K. We note that the performance indices are $P_3 > 0.995$ for each month. Therefore, we determine use of the three principal components for approximating the omnidirectional color signals. Moreover, the principal components for the omnidirectional scenes through one year were computed from the whole data sets of five months. The performance index of this case is depicted also in Fig. 10.

As a result, the omnidirectional color signals for all seasons can be represented using three common principal components. Figure 11 shows the spectral curves of the three principal components for all omnidirectional scenes. With these spectral curves, the color signals can be estimated as

$$\hat{\mathbf{e}}_3(\theta,\phi) = c_1(\theta,\phi)\mathbf{u}_1 + c_2(\theta,\phi)\mathbf{u}_2 + c_3(\theta,\phi)\mathbf{u}_3. \qquad (6)$$

It is important to note that $\{\mathbf{u}_1, \mathbf{u}_2, \mathbf{u}_3\}$ are common for all seasons. In comparison of Fig. 11 with Fig. 5, we note that the second and third components look reversed. The order of the second and third can change places in the individual seasons. The three component curves obtained from the color signal database in Fig. 5 appear to corresponding to the winter season rather than to the real scene.

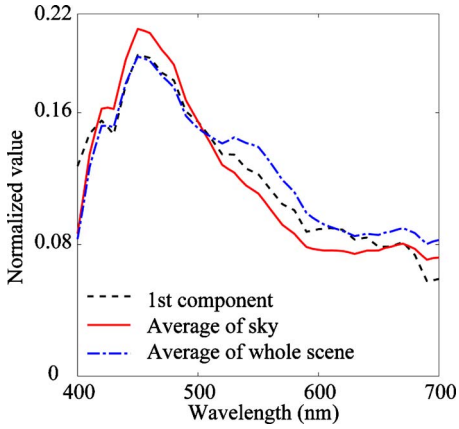

Figure 12. Comparison of the first component with the mean spectra of the sky area and the whole scene in August.

In order to confirm the reliability of the proposed method, we have estimated the spectral-power distributions of color signals in a linear combination of the three spectral bases. The estimation accuracy was examined for the eight areas shown in Fig. 7. The fourth and fifth columns in Table III list the RMSE and the ΔE^*ab between the estimated color signals by the three spectral bases in Fig. 9 and the direct measurements. Note that the estimation accuracy does not essentially deteriorate as compared with the original estimation accuracy.

Chromaticity Characteristics

The first principal component is closely related to the mean spectrum of the whole scene. Although light intensities in an outdoor scene range quite widely from shadow areas to bright light source areas, most of the brightest areas in the present campus scene are considered the sky area. That is, the sky area contributes most as light sources to object surfaces at the particular point. For instance, the first principal component of August is shown in Fig. 9(a). Then we extract the sky area from the omnidirectional image of August in Fig. 3(b). Figure 12 compares the first component with the mean spectra of the sky area and the whole scene. The fist principal component curve is close to the average of the whole scene so that the sky contributes the first component. Figure 13 depicts the chromaticity distribution of the sky area on the CIE-*xy* diagram. The chromaticity coordinates of every pixel in the sky area is plotted with a small open circle. An arrow indicates the chromaticity of the first principal component. This chromaticity is close to the Planckian locus. On the other hand, the chromaticity coordinates of the sky area vary widely, although the distribution follows roughly along the locus.

Figure 14 shows the chromaticity histogram of the omnidirectional color signals in April and August. The number of pixels with the same chromaticity is represented as the color level. The gradation from red to green means a decrease in the number of pixels with the same chromaticity. The chromaticities are not necessarily coincident with the Planckian locus, but widely distributed. This is because the chromaticity distribution is influenced not only by the direct

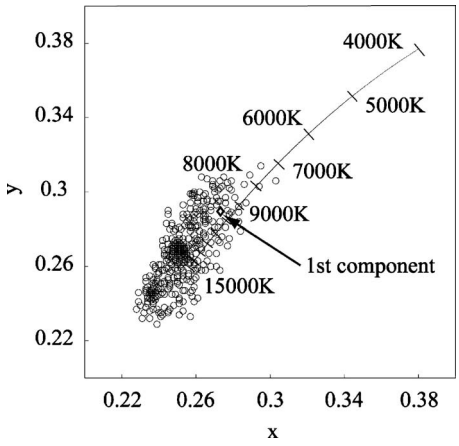

Figure 13. Chromaticity distribution of the sky area in August scene on the CIE-*xy* diagram.

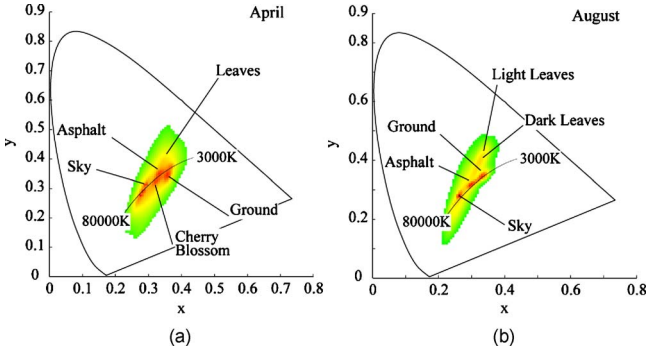

Figure 14. Chromaticity histogram of the omnidirectional color signals. (a) April and (b) August.

illumination from the sky but also by the indirect lights reflected from various object surfaces. The spring image in Fig. 3(a) includes road trees of cherry blossoms. The color of cherry blossoms is projected onto the chromaticity diagram. Green leaves in August are reflected in the chromaticity histogram in Fig. 14(b)

Image Rendering

The omnidirectional images for all seasons can be rendered using only three spectral components. Figure 15 shows the omnidirectional color images in five months, which were rendered by Eq. (6) using only the three principal components in Fig. 11. These images are almost completely coincident with the original images. For instance, the image in Fig. 15(b) looks complexly the same as the original in Fig. 7. From a data compression standpoint, we use only three numerical values for the coefficients $\{c_1, c_2, c_3\}$ at each pixel. Because the same spectral bases are used for all omnidirectional color signals, high data compression can be achieved.

The omnidirectional color signals discussed in this article are useful for image rendering in natural environment. We can render any objects as if it is placed in the real scene. Figure 16(a) shows an example of a mirrored ball which was rendered using the compressed data of omnidirectional color signals obtained from our university campus in February. The mirrored ball and the black pole are virtual objects. The

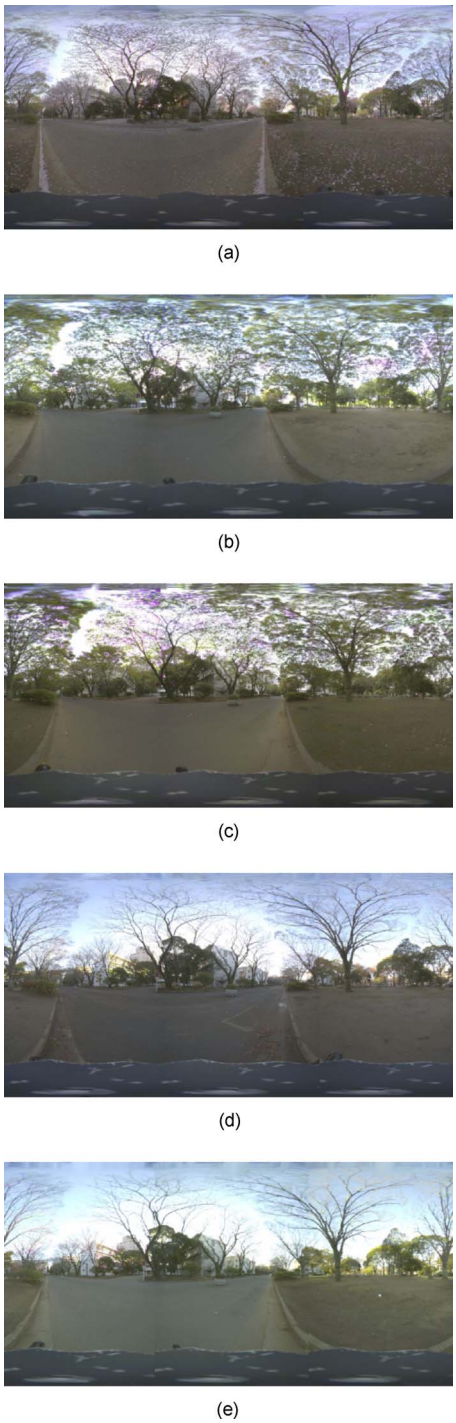

Figure 15. Omnidirectional color image rendered using only three principal components. (a) April 4, 2008, (b) August 6, 2008, (c) October 4, 2008, (d) December 3, 2008, and (e) February 6, 2009.

background is the recovered scene from the estimated color signals. The material of the ball was assumed to be polished stainless steel. The surface reflection was described using the Cook–Torrance model.[19] Then, a ray-tracing algorithm was adopted for image rendering by tracing imaging rays of light from a viewpoint to the ball in the scene.[20] The ball in Fig. 16(a) is illuminated from all directions with various light sources, consisting of the reflected light from surrounding objects and the direct light from the sky. We note that

(a)

(b)

Figure 16. Comparison between the rendered image of a mirrored ball in the scene and the real photograph: (a) image rendered using the compressed data of omnidirectional color signals in February; (b) real photograph of the ball in the same scene taken 30 min later.

the surrounding scene is specularly reflected on the ball surface. Fig. 16(b) shows a real photograph of the ball in the same scene. We took the photograph using a high resolution camera with a standard lens of the focal length 50 mm, 30 min after the omnidirectional imaging with a fisheye lens. Note that the photographer is clearly reflected on the surface of the mirrored surface. The rendered image in Fig. 16(a) appears close to this real image.

CONCLUSION

This article has described a method for analyzing omnidirectional color signals in a natural scene, which contains direct illuminations of daylights and indirect illuminations of the reflected lights from different object surfaces. A multiband omnidirectional imaging system was used for capturing high resolution images in the omnidirectional observations at a particular point in a natural scene. The spectral-power distributions of color signals were recovered from the captured six-band images. The spectral composition of the omnidirectional illumination was investigated based on the PCA in detail. We examined the omnidirectional color signals acquired at the same location in a fixed time of day in five months of a year. It was found that all the omnidirectional color signals could be expressed in a linear combination of only three principal components. Because the data volume of omnidirectional color signals is huge, this property has the potential for high data compression. Moreover, we analyzed the chromaticity distribution of omnidirectional color signals. Experimental results were presented for omnidirectional color signals obtained in an outdoor scene of a university campus. The reliability of the proposed analysis method was confirmed from various points of view. As an application, the three spectral components were useful for image rendering in a natural environment.

In this article, the omnidirectional color signals were analyzed based on the multispectral images captured at a fixed time in the five days of different seasons. The spectral analysis of image sequence captured at different times of day remains as our future work.

ACKNOWLEDGMENTS

The authors would like to thank Keita Hirai for help in creating the color signal databases. This work was presented in part at the 2009 Gjϕvik Color Imaging Symposium, Gjϕvik, Norway.

REFERENCES

[1] C. C. Chiao, T. W. Cronin, and D. Osorio, "Color signals in natural scenes: Characteristics of reflectance spectra and effects of natural illuminants", J. Opt. Soc. Am. A **17**, 218 (2000).
[2] C. C. Chiao, D. Osorio, M. Vorobyev, and T. W. Cronin, "Characterization of natural illuminants in forests and the use of digital video data to reconstruct illuminant spectra", J. Opt. Soc. Am. A **17**, 1713 (2000).
[3] J. Romero, A. García-Beltrán, and J. Hernández-Andrés, "Linear bases for representation of natural and artificial illuminants", J. Opt. Soc. Am. A **14**, 1007 (1997).
[4] J. Hernández-Andrés, J. L. Nieves, E. M. Valero, and J. Romero, "Spectral-daylight recovery by use of only a few sensors", J. Opt. Soc. Am. A **21**, 13 (2004).
[5] J. Hernández-Andrés, J. Romero, J. L. Nieves, and R. L. Lee, Jr., "Color and spectral analysis of daylight in southern Europe", J. Opt. Soc. Am. A **18**, 1325 (2001).
[6] E. M. Valero, J. L. Nieves, S. M. C. Nascimento, K. Amano, and D. H. Foster, "Recovering spectral data from natural: Scenes with an RGB digital camera and colored filters", Color Res. Appl. **32**, 352 (2007).
[7] O. Kohonen, J. Parkkinen, and T. Jääskeläinen, "Databases for spectral color science", Color Res. Appl. **31**, 381 (2006).
[8] D. B. Judd, D. L. MacAdam, and G. W. Wyszecki, "Spectral distribution of typical daylight as a function of correlated color temperature", J. Opt. Soc. Am. **54**, 1031 (1964).
[9] E. L. Krinov, *Spectral Reflectance Properties of Natural Formations: Technical Translation TT-439* (National Research Council of Canada, Ottawa, 1947).
[10] L. T. Maloney, "Evaluation of linear models of surface spectral reflectance with small numbers of parameters", J. Opt. Soc. Am. A **3**, 1673 (1986).
[11] J. P. S. Parkkinen, J. Hallikainen, and T. Jaaskelainen, "Characteristic spectra of Munsell colors", J. Opt. Soc. Am. A **6**, 318 (1989).
[12] M. J. Vrhel, R. Gershon, and L. S. Iwan, "Measurement and analysis of object reflectance spectra", Color Res. Appl. **19**, 4 (1994).
[13] P. E. Debevec, "Rendering synthetic objects into real scenes", *Proc. SIGGRAPH 98* (ACM, New York, 1998) p. 189.
[14] R. Dror, A. S. Willsky, and E. H. Adelson, "Statistical characterization of real-world illumination", J. Vision **4**, 821 (2004).
[15] S. Tominaga and N. Tanaka, "Omnidirectional scene illuminant estimation using a mirrored ball", J. Imaging Sci. Technol. **50**, 217 (2006).
[16] S. Tominaga, T. Fukuda, and A. Kimachi, "A high-resolution imaging system for omnidirectional illuminant estimation", J. Imaging Sci. Technol. **52**, 040907 (2008).
[17] N. Shimano, "Recovery of spectral reflectances of objects being imaged without prior knowledge", IEEE Trans. Image Process. **15**, 1848 (2006).
[18] G. Wyszecki and W. S. Stiles, *Color Science: Concepts and Methods, Quantitative Data and Formulae* (Wiley, Hoboken, NJ, 1982), Chap. 1.
[19] R. Cook and K. Torrance, "A reflection model for computer graphics", *Proc. SIGGRAPH 81* (ACM, New York, 1998) p. 307.
[20] R. Hall, *Illumination and Color in Computer Generated Imagery* (Springer-Verlag, New York, 1988).